Acta Cryst. (1998). A**54**, 675–681

Stable Desmearing of Slit-Collimated SAXS Patterns by Adequate Numerical Conditioning

M. Soliman,[a] B.-J. Jungnickel[a]* and E. Meister[b]

[a]*Deutsches Kunststoff-Institut, Darmstadt, Germany, and* [b]*Technische Universität Darmstadt, Fachbereich Mathematik, Darmstadt, Germany. E-mail: bjungnickel@dki.tu-darmstadt.de*

(*Received 11 December 1997; accepted 20 April 1998*)

Abstract

Small-angle X-ray scattering (SAXS) patterns from slit cameras ('Kratky cameras') require a subsequent desmearing procedure in order to obtain the pinhole scattering curve that is suitable for subsequent structure analysis. Since the corresponding integral equation contains a singularity, its solutions are usually unstable and fail if large noise is present. It is demonstrated how analytical stability can be achieved by physically reliable conditioning of the experimental data, introduction of the Moore–Penrose pseudoinverse of the equation's discretized integral operator and solving the equation by a FFT algorithm. This ensures the consistency of the solution as well as its stability, and hence its convergence. This solution can account for arbitrarily nonsymmetrical primary-beam profiles. The algorithm does not require antecedent smoothing of the scattering curve. It allows on the contrary low-pass filter smoothing during desmearing but remains stable despite large noise contributions.

1. Introduction

Structure analysis of biological objects or of polymers often requires investigations on the length scale of 1–100 nm. Then, small-angle X-ray scattering (SAXS) is a powerful and widely used tool since, using Cu $K\alpha$ radiation ($\lambda \approx 0.154$ nm), Bragg angles 2θ will be less than 5° (Glatter & Kratky, 1982). The low scattering power of the light elements in such materials yields, however, at point collimation of the primary beam weak scattering patterns. The problem is usually overcome by use of slit cameras as suggested first by Kratky (1954) ('Kratky camera'), where a collimated parallel primary beam is used with a length (coordinate u) of several centimetres and an intensity distribution $I_p(u)$ (Fig. 1) (Glatter & Kratky, 1982; Kratky, 1954). Such an experimental procedure, however, almost always requires a defolding step ('desmearing') in order to get that (pinhole) intensity pattern $I_0(s)$ from the experimental one $I_{\exp}(s)$ that then allows further evaluation during structure analysis. The introduced functions are related by (Glatter & Kratky, 1982; Kratky, 1954; Strobl, 1970)

$$I_{\exp}(h) = \int_{-\infty}^{+\infty} V(u') I_0[(h^2 + u'^2)^{1/2}]\,\mathrm{d}u', \qquad (1)$$

where

$$V(u') = \int_{u'-w}^{u'+w} I_p(u)\,\mathrm{d}u \qquad (2)$$

with the width $2w$ of the counter window and

$$h = D\tan[\arcsin(s\lambda/2)] \qquad (3a)$$

$$s = 2\sin\theta/\lambda, \qquad (3b)$$

where s is the scattering vector, h and u' are the geometrical coordinates perpendicular and parallel to the primary beam, respectively, in the registration plane, and D is the sample–registration-plane distance. These relations are easily derived from Fig. 1. Considering that $h^2 + u'^2 = b^2$ and defining

$$G(x) = [V(x^{1/2}) + V(-x^{1/2})]/2x^{1/2}, \quad G(x) \equiv 0 \text{ at } x \leq 0, \qquad (4)$$

equation (1) can be rewritten, following Strobl (1970), as

$$I_{\exp}(h) = \int_{h^2}^{\infty} G(b^2 - h^2) I_0(b)\,\mathrm{d}b^2 = \mathcal{G} I_0(h), \qquad (5)$$

where $\mathcal{G}$ is the corresponding integral operator. Equation (5) relates, *via* the geometrical scattering condition as expressed by G, the experimental intensity distribution $I_{\exp}$ to the pinhole intensity function I_0 and, for further structure analysis, must be solved for the latter. This is not a trivial problem since, by virtue of $G(x) = G[V(x), x]$, the integrand of the integral in (5) approaches infinity somewhere in the domain of integration, *i.e.* it contains a singularity at $b^2 = h^2$ or $G(x = 0)$. The singularity is introduced by the coordinate transformation (4), which, however, transforms equation (1) into the easily tractable linear convolution equation (5). Deconvolution and, therefore, solving the problem would, in principle and disregarding the singularity for the moment, be possible by the Fourier transformation technique if the range of integration could be suitably adapted. Then,

$$I_0[(b^2)^{1/2}] = \mathcal{F}^{-1}\left\{\frac{\mathcal{F}[I_{\exp}(b^2)]}{\mathcal{F}[G(b^2-h^2)]}\right\}, \qquad (6)$$

where $\mathcal{F}$ designates the Fourier transformation, would be a solution of (5). In fact, the singularity prohibits such a procedure.

Owing to the mentioned singularity, numerical algorithms to solve integral equations like (5) often yield unstable solutions $I_0(h)$, which means that small errors in $I_{\exp}$ may cause large errors in I_0. This can be caused by the noise in measured scattering patterns. In addition, discretization errors may arise and a finer discretization does not necessarily result in a more reliable solution (Louis, 1981). These errors may become obvious by 'dips' in the calculated pinhole scattering function I_0 or can sometimes even cause 'negative' intensities or non-existent peaks in I_0. The term 'ghosts' summarizes these phenomena (Louis, 1981). All this may indicate non-existing structural features.

The spectral decomposition, *i.e.* the Fourier transform $\mathcal{F}\{\mathcal{G}\}$, of the integral operator $\mathcal{G}$ [equations (4) and (5)] can be directly computed from the geometrical scattering conditions. It is known that Fourier transforms are nonsensitive to singularities in their stem functions. If those spectral components of the inverse $\mathcal{G}^{-1}$ of $\mathcal{G}$ that are linked to the singularity behaviour of G, *i.e.* those with the highest amplitude, are suppressed, the so-called 'Moore–Penrose pseudoinverse' $\mathcal{G}^{*-1}$ (Penrose, 1955; Golub & van Loan, 1995) is obtained. Its use instead of $\mathcal{G}^{-1}$ during subsequent calculations would therefore make the solution algorithm stable. Then, a finer discretization would yield a better solution.

In the present paper, it will be shown that the named problems can all be avoided, and a stable solution of the desmearing problem can be found by use of the integral equation $I_{\exp}(I_0)$ in its convolution form [equation (5)]. In (5), $G(0)$ is replaced by a physically reliable value, which ensures the consistency of the solution and such energy conservation. Finally, the Moore–Penrose pseudoinverse of the equation's discretized integral operator is introduced, and (5) is solved for I_0 by a fast Fourier transform algorithm according to (6).

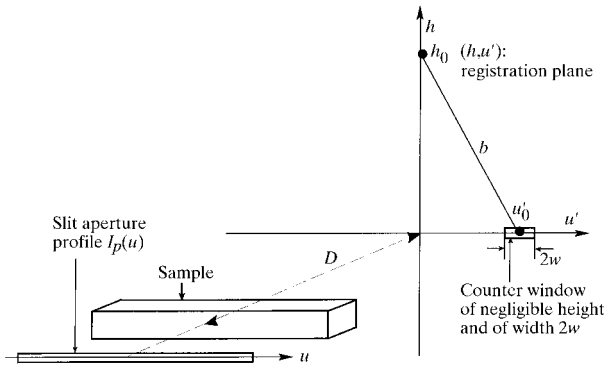

Fig. 1. Geometry of slit-collimated small-angle X-ray scattering and definition of coordinates. D: distance sample–registration plane.

2. Theoretical preliminaries

2.1. *Overview on introduced concepts*

Mazur & Wims (1966) derived for (5) the analytical solution

$$I_0(h) = \int_0^\infty \{I_{\exp}[(u'^2+h^2)^{1/2}]F(u')/\pi(u'^2+h^2)^{1/2}\}\,\mathrm{d}u', \qquad (7)$$

where Green's function $F(u')$ is the solution of the Volterra equation of the second kind,

$$F(u') + (2u'/\pi)\int_0^{u'} F(z)K[(u'^2-z^2)^{1/2}]\,\mathrm{d}z = 1 \qquad (8)$$

and

$$K(z) = \frac{1}{z}\int_0^1 \frac{x[\mathrm{d}V(zx)/\mathrm{d}(zx)]\,\mathrm{d}x}{(1-x^2)^{1/2}}. \qquad (9)$$

This approach avoids the mentioned singularity by an additional integration, this being equivalent to a distribution of the singularity over a finite range. Such, however, an additional smearing step and the additional problem of solving equation (8) are introduced.

Strobl (1970), whose approach seems to be the most commonly used, calculated Green's function of (5) for a trapezoidal $I_p(u)$. The calculation of Green's function is equivalent to the calculation of the inverse matrix of the discretized $\mathcal{G}$. The resulting matrix is ill conditioned since G is singular (Strobl, 1970; Prössdorf & Silbermann, 1991; Golub & van Loan, 1995). This is the reason for occasional artefacts like the already mentioned ghosts that adulterate the solution. The reliability of the solution can be enhanced by suitable numerical measures but the computational effort rises considerably and the basic problem, *i.e.* the instability of the solution, remains. The condition number $c_\infty \sim 1/d$ (Strobl, 1970) (d is the discretization step width of both G and $I_{\exp}$ as chosen by the program) diverges for that algorithm with finer discretization, which indicates instability and nonconvergence.

Fedorov *et al.* (1969) solved the problem by transforming the integral equation into an expression like $(\mathcal{E}-\mathcal{A})I_0 = I_{\exp}$, where $\mathcal{E}$ is the unity operator and the operator $\mathcal{A}$ results from $I_p(u)$ by suitable differentiations. In some Hilbert norm, it can be assured that $\|\mathcal{A}\| < 1$ and the equation can be solved using a Neumann series ($I_0 = \sum_{n=0}^\infty \mathcal{A}^n I_{\exp}$). The already described problems arise again since the discretized $\mathcal{A}$ tends to have eigenvalues greater or equal to unity (this in turn violates the condition $\|\mathcal{A}\| < 1$ for the discretized

problem). Those eigenvalues belong to eigenvectors that can again produce the already mentioned artefacts.

Many more attempts to treat the problem can be found in the literature (*e.g.* Guinier & Fournet, 1947; Lake, 1967; Ruland, 1964; Hossfeld, 1968). Their closer inspection reveals that they all suffer from the same problem, that is the lack of stability of the solution, which arises from the singularity of the underlying integral equation.

2.2. *Nature and mathematical origin of ghosts*

In Fig. 2, a hypothetic pinhole scattering curve $I_0(s)$ is shown together with its smeared counterpart $I_{\exp}(s)$. The latter has been desmeared twofold $[I_0'(s)]$ according to Strobl (1970), assuming the intensity distribution along the slit is trapezoidal. In one of these two examples, an improper effective accuracy measure $\varepsilon_S \sim c_\infty c_R$ (c_R is the condition number contributions of the implemented Gauss algorithm, the singularity discretization and others) has been chosen. It can easily be seen how $I_0(s)$ differs then from $I_0'(s)$ and that coincidence is improved by increase of the computational effort by *e.g.* finer discretization near the singularity. The features as marked by arrows are the already mentioned ghosts, *i.e.* blurred side images of the peaks in the original curve.

From (5), it can be concluded that the observed intensity at a position h is influenced only by contributions of the pinhole intensity function for which $b > h$. Discretized integral operators $\mathcal{G}$ and, hence, $\mathcal{G}^{-1}$ will then be of upper right triangle form (Cramer's rule). Moreover, owing to the singularity of G at $b = h$, $I_{\exp}(h)$ is predominantly determined by $I_0(b)$. This is illustrated by Fig. 3(*a*), where the smeared intensity pattern is shown for a δ-like pinhole scattering function, $I_0(b) = \delta(b - b_0)$, and a symmetrically trapezoidal slit intensity distribution. Then, $I_{\exp}(h) = 2b_0 G(b_0^2 - h^2)$. If, by erroneous discretization upon numerical evaluations, the weight of the singularity of G is too low, G will be somewhat broadened. An observed decay of $I_{\exp}(h)$ can then only be satisfied by a discretized function $I_0(b)$ with values smaller than those of the right solution (including occasionally even negative values) for some b. Such an 'undershot' or 'dip' is one kind of the already introduced 'ghosts' and can erroneously be interpreted as a structural feature. Overestimating the singularity's weight of G, in contrast, will in an analogous manner give an overshot, *i.e.* another kind of ghost. The cited desmearing approaches will therefore nevertheless work well if the X-ray intensity profile under consideration is a strictly monotonous falling function or does not contain narrow peaks lying closely together.

3. Conditioning of experimental data

It is well known that Fourier transformation transforms peaks or singularities into broad nonsingular courses and distributes them over the whole definition range of the stem function. It is moreover assumed that the Fourier discretization errors are negligible with respect to the Fourier integral weight of the singularity. In order to obey the latter condition and to make the Moore–Penrose truncation tractable, the numerical Fourier transformation must be performed in a suitable manner. At first, one of the transformation's integration sampling points is placed exactly at the singularity, *i.e.* at $b^2 - h^2 = 0$. Then, during discrete Fourier transformation, for the diverging $G(0)$ another value $G^*(0)$ is used, which nevertheless yields the right value of $\mathcal{F}\{G\}$ at least at that space frequency k that is dominant for desmearing. This will ensure consistency of the solution. This particular space frequency is $k = 0$ as can be derived from the following considerations. It follows from (5) that

$$\int I_{\exp}(h)\,\mathrm{d}h = \int G(h)\,\mathrm{d}h \int I_0(h)\,\mathrm{d}h. \tag{10}$$

This expresses the energy conservation during smearing since on both sides of the equation are integral scattered intensities and the integral pinhole intensity $I_0(h)$ is normalized by the integral illumination strength. It is moreover

$$\int I_{\exp}(h)\,\mathrm{d}h = \int I_{\exp}(h)\exp(ikh)\,\mathrm{d}h\big|_{k=0} = \mathcal{F}\{I_{\exp}\}\big|_{k=0}. \tag{11}$$

The space frequency $k = 0$ in the Fourier transform reflects therefore the integrated scattered intensity and, therefore, dominates the desmearing. The procedure to find the proper $G^*(0)$ is described below. Finally, since the slit and, consequently, I_p are of finite length, there must be a value $B_q/2$ such that $G(b^2 - h^2) \equiv 0$ for $b^2 - h^2 \geq B_q/2$. This allows replacement of the limits of integration in (5) by $\pm B_q/2$. Moreover, we set $G(x) = 0$ for $x \in [-B_q, 0] \cup [B_q/2, B_q]$ (*cf.* Fig. 3*b*). The range of integration is then arbitrarily broadened to B_q since then, for no value of $b^2 - h^2 \geq B_q$ can the values of $I_0(b^2 - h^2)$ affect $I_{\exp}(h)$ and *vice versa*. Now, a periodical representation of $I_{\exp}$, I_0 and G over $\pm B_q$ is possible. By these means, moreover, the truncation errors can be eliminated since the domain of integration is finite. This all allows a 'fast Fourier transformation' (FFT) technique without disturbing the values of I_0 in the domain of interest, *i.e.* $b^2 \in [0, B_q/2]$ (Prössdorf & Silbermann, 1991). In order to meet the usual convention, the coordinate transformation $x \to y = Fx/2B_q$ should be made where $F \in 2^N$ (N integer) is the number of FFT sampling points in these new coordinates. This transforms the FFT sampling points to integer positions. $I_0(h)$ can then be calculated according to

$$I_0(h^2) = \frac{1}{2B_q}\mathrm{FFT}^{-1}\left(\frac{\mathrm{FFT}\{I_{\exp}[(b^2 - h^2)^{1/2}]\}}{\mathrm{FFT}^{-1}[G(b^2 - h^2)]}\right). \tag{12}$$

Care has to be taken to translate this formal equation during numerical calculations correspondingly. In the

denominator of equation (12), the back transformation instead of the forward transformation must be used since, following Strobl (1970), the argument $b^2 - h^2$ has been chosen for G instead of $h^2 - b^2$. The FFT can be performed by the usual Butterfly algorithm (van Loan, 1992).

In order to evaluate (12), as announced, a substitute G_0^* for $G_0 = G(b^2 \rightarrow h^2)$ has to be determined that can

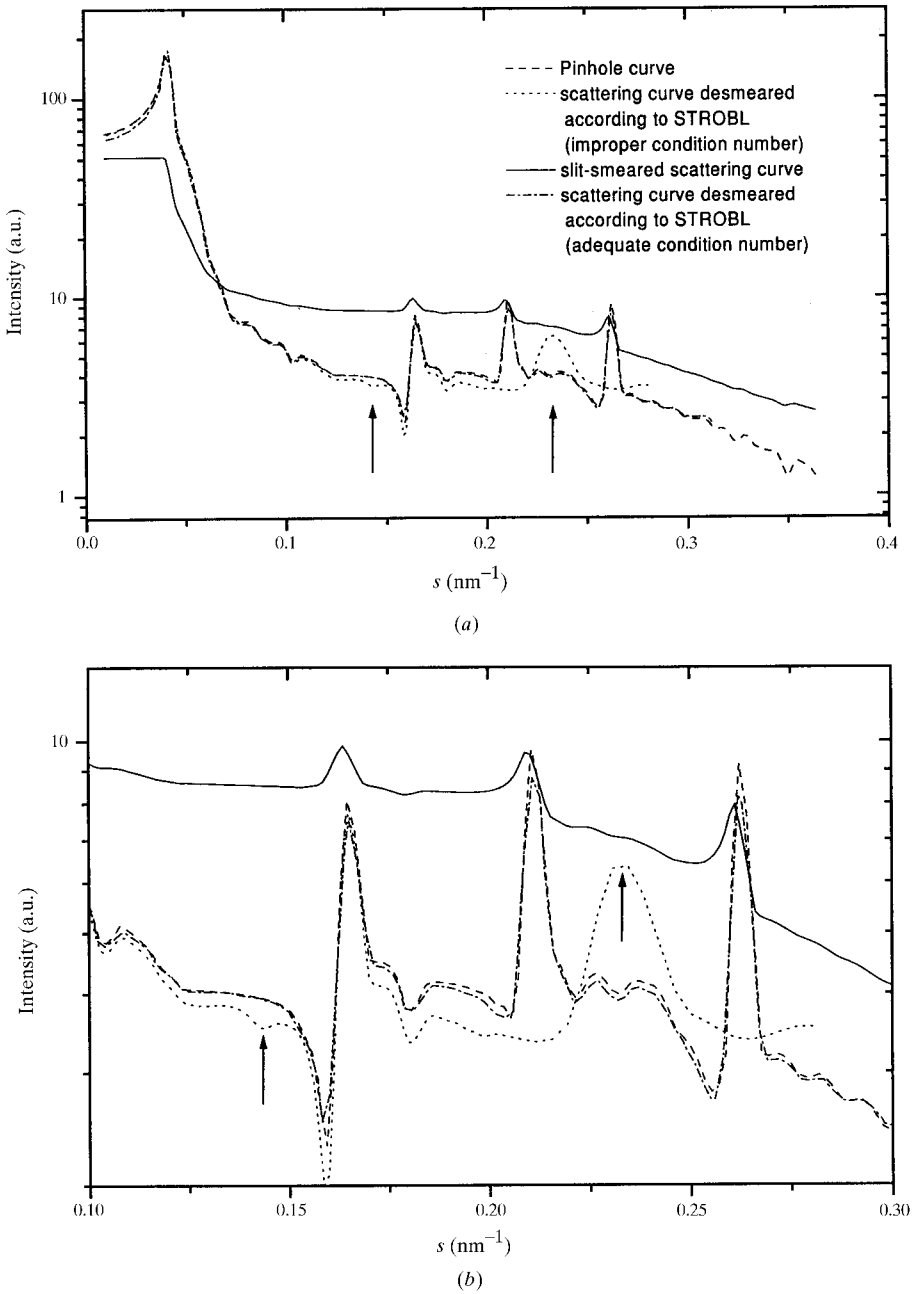

Fig. 2. Comparison of a hypothetical pinhole scattering curve with its experimental counterpart as slit-smeared with a symmetrically trapezoidal primary beam and desmeared according to Strobl (1970). An improper effective accuracy ε_S, that is, a too fine discretization of G and I_{exp} in the computational version of that algorithm, causes some 'ghosts' as marked by arrows. However, modelling the original curve is improved by choosing an adequate ε_S and enlarging the computational effort. The desmeared scattering curve as obtained by the present algorithm coincides completely with the original pinhole curve and, within this figure, cannot be distinguished from it. Grid size: 200 measuring points in the measuring range of $\Delta s = 0.36$ nm^{-1} for the Strobl curve and 32 768 ($= 2^{15}$) for the present algorithm. (*a*) Complete curves, (*b*) center parts [meaning of symbols as in (*a*)].

be introduced into the $\mathrm{FFT}^{-1}[G(b^2-h^2)]$. As G is defined to vanish for all $b^2-h^2<0$, and, for $b^2-h^2>0$, $G(b^2-h^2)\to\infty$ as $b^2-h^2\to 0$, two different values for G_0 have to be introduced: $G_0^- = \lim_{0>b^2-h^2\to 0} G(b^2-h^2)$ and G_0^+ as a formal substitute for G_0 on the side $b^2-h^2>0$. Here, $G_0^-=0$ is set since $G=0$ for all $b^2-h^2<0$. In the new y coordinates, it is $y_l = l$ and therefore

$$\begin{aligned}\mathrm{FFT}^{-1}[G](k_n) &= \sum_{l=(-F/2),l\neq 0}^{F/2-1} G_l \exp(-ik_n l) \\ &\quad + (G_0^+ + G_0^-)/2 \\ &= \sum_{l=1}^{F/2-1} G_l \exp(-ik_n l) + G_0^+/2, \end{aligned} \tag{13}$$

since by definition $G_l = 0$ for $l<0$ and $G_l = G(y_l) = G(l)$. Since, for a trapezoidal $I_p(u)$, $G(x)$ near $x=0$ behaves as $O(1/x^{1/2})$ [*cf.* equation (4)] and its Fourier transform behaves accordingly, $\mathrm{FFT}^{-1}[G](k_n=0)$ has the highest weight in (13). G_0 is approximated from (13) with $n=0$ and the two-point integration as performed by the FFT between $l=0$ and $l=1$:

$$[G_0^* + G(1)]/2 \approx \int_0^1 G(l)\,\mathrm{d}l + O(F^{-1}). \tag{14}$$

Going back to the original coordinates, we have

$$G_0^* = (F/B_q)\int_0^{2B_q/F} G(\xi^2)\,\mathrm{d}\xi^2 - G(2B_q/F). \tag{15}$$

Together with equation (4), one finally obtains

$$G_0^* = (F/B_q)\int_{-(2B_q/F)^{1/2}}^{(2B_q/F)^{1/2}} V(z)\,\mathrm{d}z - G(2B_q/F). \tag{16}$$

The evaluation of the remaining integral is straightforward. It easily allows also consideration of nonsymmetrical primary-beam profiles that can be due to bad adjustment of the X-ray camera. Equation (16) now yields a G_0^* that permits introduction of an $\mathcal{F}\{G\}$ into (12) without causing singularity problems.

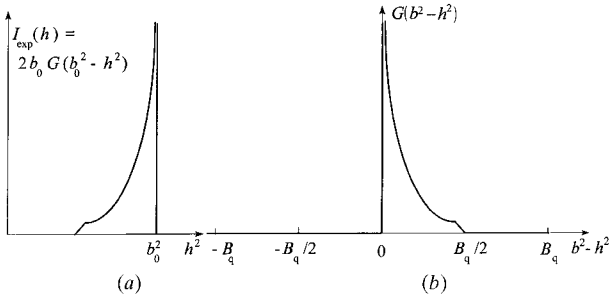

Fig. 3. (*a*) Slit-smeared scattering curve of a δ-like pinhole scattering at b_0 for a symmetrically trapezoidal primary beam. (*b*) Definition of the integration interval for the Fourier transformation as illustrated by the smeared scattering curve of (*a*).

Finally, the Moore–Penrose inversion is accomplished directly within the division by $\mathrm{FFT}^{-1}[G](k_n)$ in (12) in the following manner. If, for some k_n, $\mathrm{FFT}^{-1}[G](k_n)$ becomes smaller than a precision limit ε to be defined by the algorithm

$$\frac{\mathrm{FFT}^{-1}[G](k_n)}{\max_{\forall k_n}\mathrm{FFT}^{-1}[G](k_n)} \le \varepsilon \tag{17}$$

[*cf.* equation (13)], the nominator of (12) is not divided by this value but multiplied by zero. ε is the product of the condition number c_2 of the algorithm

$$c_2 = \sigma_{\max}/\sigma_{\min}, \tag{18}$$

where $\sigma_{\max}$ and $\sigma_{\min}$ are the largest and smallest absolute values of $\mathcal{G}$'s eigenvalues and the machine precision (*i.e.* essentially the precision remaining for calculations). It remains limited for all d in contrast to that which rules the Strobl (1970) algorithm. This ensures analytical stability. As expressed by equation (17), ε is chosen such that those spectral components of $\mathcal{G}$ are cancelled whose weight after division would exceed the number of their reliable digits normalized by the value of the most reliable spectral component. By suitable choice of ε, also those spectral components that have numerical noise can be eliminated. This, in fact, was one of the initial aims of the Moore–Penrose inversion (Penrose, 1955). Use of a small ε or c_2 is equivalent to the introduction of a low-pass filter.

4. Discussion and concluding remarks

It has already been pointed out that the introduced desmearing concepts work well for scattering curves with monotonically falling course or if only broad well separated maxima are present. They require, however, if working at all, high computational efforts if the named conditions are not fullfilled. Computation time and memory need increase usually like N^2 ($N\sim 1/d$ is the sampling point number) as, *e.g.*, for the Strobl (1970) algorithm because that is based essentially on a Gauss algorithm. In contrast, the time and memory needs of the present algorithm increase proportional to $N\ln N$ and N, respectively, for sufficiently large N as known for FFT routines. The reliability of our algorithm is demonstrated by Fig. 2 where the original pinhole curve and that desmeared according to the present algorithm curve coincide within machine precision. It is moreover easy to consider arbitrary courses of the primary-beam profile including nonsymmetric ones. This reduces the demands on the adjustment of the X-ray camera.

It should be pointed out that the conventional desmearing procedures work with a limited number of sampling points (usually about 200). A finer discretization causes their failure owing to the instability if noise

contributions are present and leads to an extreme increase in computational effort. The present algorithm, on the contrary, allows the use of a huge number of sampling points with acceptable computational time and memory as well. The curves of Fig. 2 have been calculated accordingly. In fact, the analytical stability of the presented algorithm is of particular importance for noisy scattering patterns. The effect of instabilities depends sensitively on the 'right' choice of the discretization grid and such a right choice is almost impossible for noisy curves. The conventional desmearing routines including the Strobl algorithm require therefore a careful

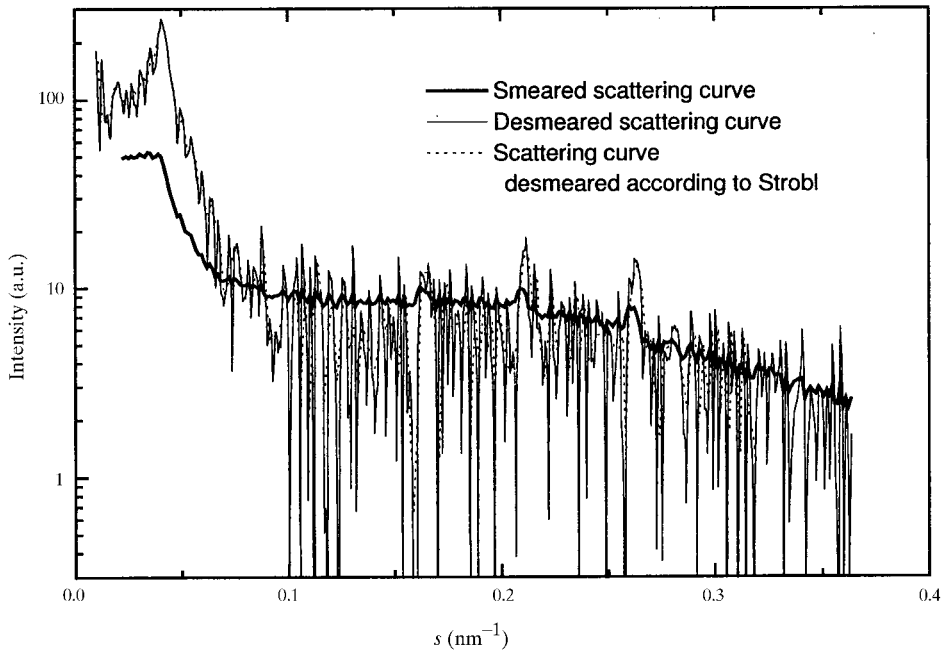

(*a*)

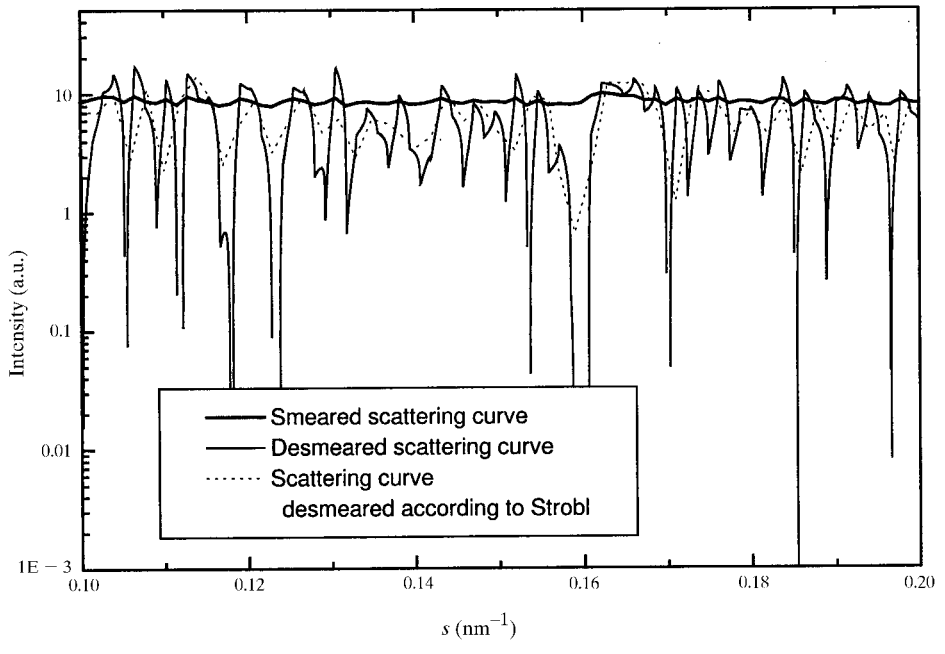

(*b*)

Fig. 4. Slit-smeared scattering curve as in Fig. 2 with superimposed noise together with the patterns as desmeared according to the present and to the Strobl algorithms. Same calculation conditions as in Fig. 2. (*a*) Complete curves, (*b*) center part.

smoothing of the scattering curves prior to desmearing. Such smoothing with equal weight for all h, on the other hand, is equivalent to a redistribution of intensity. This violates energy conservation for that part of the noise, which stems from the X-ray source. This noise must be distinguished from the noise of the electronics, and the distinction of the two contributions is, in principle, possible if the power spectra are known (the X-ray source noise, for example, obeys a Poisson distribution). Owing to the stability of our algorithm, smoothing can be performed during or even after desmearing without failure of the procedure. Clearly, it cannot be prevented that nonscattering contributions to I_{exp} cause occasionally negative intensities. However, these negative peaks either bear only a negligible amount of intensity and correspond to easily removable high-frequency spectral components of I_0 or result from statistical errors which mimic structure and can be eliminated by increasing the measuring time. In principle, these problems could be overcome in the frame of the present algorithm by performing smoothing during desmearing by, *e.g.*, application of a low-pass filter on the Fourier transform of I_{exp}. This could be performed by proper choice of ε as outlined above but such a procedure can cause another type of artefact known as Fourier truncation error.

These considerations are illustrated by Fig. 4, which displays the slit-smeared scattering curve of Fig. 2 with a superimposed noise and the corresponding calculated pinhole curves. It can clearly be seen that the present algorithm reproduces all noise peaks of the smeared curve adequately in the desmeared pattern owing to its fine discretization, whereas the conventional calculation yields an irregular and arbitrary translation of noise from which no conclusions on the physics behind it can be drawn.

It can be summarized that the proposed solution for the desmearing problem of X-ray small-angle scattering patterns from slit cameras is consistent and stable from an analytical point of view. Its numerical conversion is fast and reliable. It can take advantage of the introduced algorithms for fast Fourier transforms. The solution can account for arbitrarily nonsymmetrical primary-beam profiles, this being of particular importance since adjustment of the camera to yield an exact trapezoidal profile can be a laboriously task. The algorithm allows moreover low-pass filter smoothing during desmearing but remains stable despite large noise contributions.

The authors can provide details of a computer program.

Financial support from the Bundesminister für Wirtschaft through the Arbeitsgemeinschaft industrieller Forschungsvereinigungen (AiF grant nos. 9877 and 10421) is gratefully acknowledged.

References

Fedorov, B. A., Andreeva, N. A., Wolokova, L. A. & Voronin, L. A. (1969). *Sov. Phys. Crystallogr.* **13**, 668–672.
Glatter, O. & Kratky, O. (1982). *Small-Angle X-ray Scattering.* London: Academic Press.
Golub, G. H. & van Loan, C. F. (1995). *Matrix Computations*, 3rd ed. Oxford: North Oxford Academic Press.
Guinier, A. & Fournet, G. (1947). *Nature (London)*, **160**, 501.
Hossfeld, F. (1968). *Acta Cryst.* **24**, 643–650.
Kratky, O. (1954). *Z. Elektrochem.* **58**, 49–53.
Lake, J. A. (1967). *Acta Cryst.* **23**, 191–194.
Loan, C. F. van (1992). *Computational Frameworks for the Fast Fourier Transform.* Philadelphia: SIAM.
Louis, A. K. (1981). *Math. Methods Appl. Sci.* **3**, 1–10.
Mazur, J. & Wims, A. M. (1966). *J. Res. Natl Bur. Stand. Sect. A*, **70**, 467–471.
Penrose, R. (1955). *Proc. Cambridge Philos. Soc.* **51**, 406–413.
Prössdorf, S. & Silbermann, B. (1991). *Numerical Analysis for Integral and Related Equations.* Series *Operator Theory – Advances and Applications*, Vol. 52. Basel: Birkhäuser.
Ruland, W. (1964). *Acta Cryst.* **17**, 138–142.
Strobl, G. R. (1970). *Acta Cryst.* A**26**, 367–375.